The axial response of fully grouted rock bolts using a distributed fiber optic sensor technique

Tyler O'Connor
Department of Civil Engineering – Royal Military College of Canada, Kingston, Ontario, Canada
Bradley Forbes, Nicholas Vlachopoulos & Mark Diederichs
Department of Geological Sciences and Geological Engineering – Queen's University, Kingston, Ontario, Canada

ABSTRACT
The primary function of rock bolts is to stabilize the weakened ground around the periphery of the tunnel by transferring the load from the weakened rock to the more stable rock deeper into the rock mass. Through the use of a fiber optic sensor technology that has been developed by the authors, axial strain along the fully grouted rock bolt can be determined at a spatial resolution of 0.65 mm. This continuous strain monitoring technique provides comprehensive and unique insight into load transfer mechanism(s). This allows for in-depth geomechanical insight with respect to the behaviour of fully grouted rock bolts with a view to optimizing the performance of such rock support elements. In particular, this paper examines the effect of embedment length based on various simulated rock grout mixtures as well as specimen/rebar sizes. This paper summarizes the methodology employed for such laboratory testing of rock bolt (rebar), and provides results for a cement-grouted sample with an embedment length of 500 mm.

RÉSUMÉ
La fonction principale des boulons d'ancrage est de stabiliser les sols affaibli à la périphérie d'un tunnel en transférant la charge du roc affaibli au roc plus stable situé en profondeur dans la masse rocheuse. Avec l'utilisation de capture par fibre optique développée par les auteurs, il est possible d'examiner la déformation axiale le long du boulon d'ancrage entièrement encastré avec une résolution spatiale de 0,65 mm. Cette technique de surveillance des déformations le long du boulon fournit, en temps réel, une vue complète et claire sur le mécanisme de transfert des charges. Cela permet de mieux comprendre le comportement géomécanique des boulons d'ancrage entièrement encastré en vue d'optimiser la performance de tels éléments d'appui. En particulier, cet article examine l'effet de la longueur d'encastrement à partir de divers mélanges de mortier dans des rocs simulés, et de la taille des échantillons / barres d'armature. Cet article résume la méthodologie employée pour des essais en laboratoire de boulons d'ancrage (barre) et fournit les résultats obtenus pour un échantillon ciment-mortier avec une longueur d'encastrement de 500 mm.

1 INTRODUCTION

Underground construction projects such as tunnels and mines have been excavated around the world for hundreds of years. One of the key aspects in the support system for any underground excavation is tendon support elements (e.g. rock bolts and cable bolts) which are designed to transfer load from the weakened rock mass around the periphery of the tunnel to more stable rock deeper into the rock mass, see Figure 1. If unsupported, the weakened rock mass creates a potential rock fall hazard which is one of the main contributors to injuries in tunnel construction (Kikkawa et al. 2015). The rock mass stability around the excavation depends primarily on three factors:

1. the pre-existing rock mass structure (i.e. joints);
2. In-situ stress field; and,
3. the disturbance of the excavation method.

One common type of tendon support is a rock bolt. Rock bolts are mainly used to stabilize the immediate rock mass; this allows the project to continue and provides a safe working environment. As a result of stabilizing the surrounding rock mass, rock bolts also restrict the confinement in conjunction with other support elements (i.e. shotcrete and steel sets) (Cruz et al. 2016).

Rock bolts have been a key component in ground support as an industry standard for almost 50 years. There are many different types of rock bolts; each designed for different ground behaviours. According to Li (2007), the most common type of rock bolt is the Fully Grouted Rock Bolt (FGRB) where the reinforcement element (rebar) is bonded to the rock along its entire length with either a cement or resin-based grout. One of the benefits of being grouted along the entire length is the corrosion protection of the rebar which adds longevity to the support element and in-turn the entire support system. Rock bolts, in general, can be installed passively or actively by tensioning the bolt during the installation. When the bolt is installed actively, it begins reinforcing the rock mass immediately. In selected instances, such as using a resin-based grout, the FGRB must be spun-tensioned during installation in order to effectively mix the two components of the resin grout.

Decades of research has been focused on understanding the load transfer mechanics of rock bolts. Windsor (1997) described the rock bolt system as being comprised of four elements, see Figure 2. Using this as a baseline model, loading cases for FGRB were derived

which can be categorized as axial loading, caused by bed dilation/separation, or shear, caused by slip along the bedding plane, see Figure 3. Li and Stillborg (1999) further developed this theory for FGRB by analyzing the forces that create the shear strength along the bolt-grout interface that is mobilized during axial loading. The three mechanisms governing the shear strength along the grout-bolt interface are adhesion, mechanical interlock and friction. Each of these mechanisms prevent slippage along the interface with each of them lost in sequence as the decoupling front travels down the length of the rock bolt.

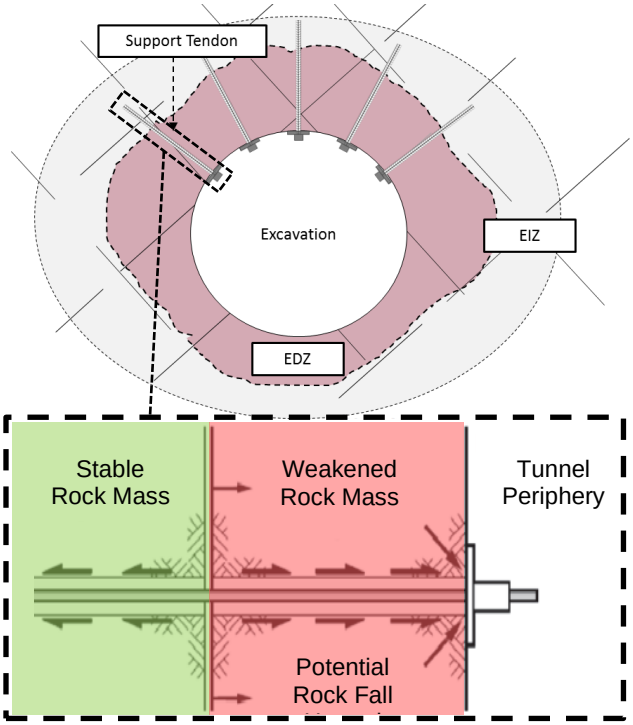

Figure 1. Top – Excavated rock mass with tendon support. (Forbes et al. 2018). Bottom – Interactions of the rock bolt components used to transfer load from unstable zone/rock to a stable zone/rock (modified Charette and Bennett 2017).

2 BACKGROUND

There has been extensive research into the axial response of rock bolts mainly through the use of pull-out tests. For example, Benmokrane et al. (1995) simulated rock by using by 60 MPa concrete cylinders to determine pull-out strength (Model A) and the relationship between bond stress and anchor slip (Model B), see Figure 4. By using concrete as a representative model of rock, there are a number of variables that led to uncertainties with the material parameters. While developing a pull-out test for cable bolts, Hyett et al. (1992) used equations to relate rock mass radial stiffness to that of steel, PVC, and aluminum

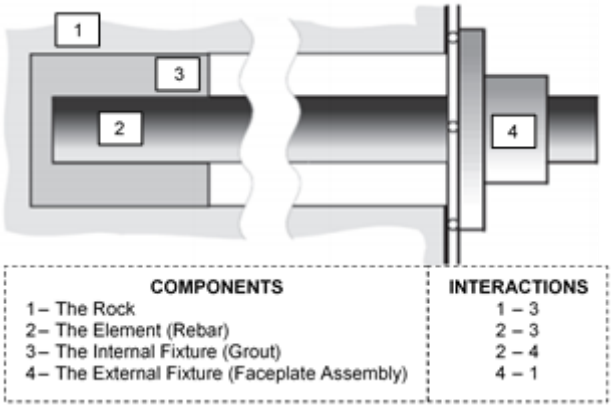

Figure 2. Load transfer components and interactions for a rock bolts (modified Windsor 1997 and Charette and Bennett 2017).

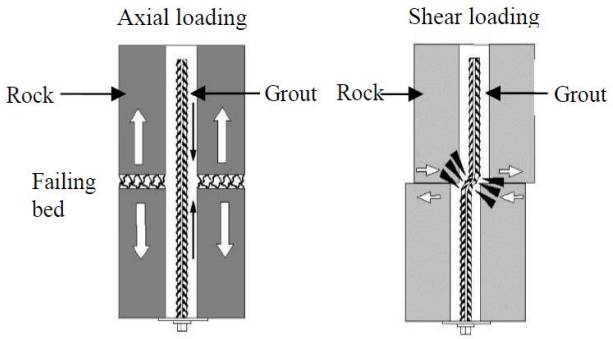

Figure 3. Loading categories for FGRB (modified Mark et al. 2002).

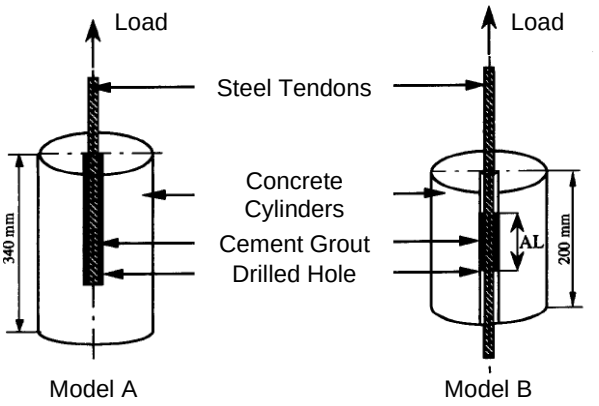

Figure 4. Fully grouted rock bolt pull-out test. Model A - Determine anchor pull-out strength as a function of the anchored length (AL). Model B – Determine the relationship between bond stress and anchor slip (modified Benmokrane et al. 1995).

pipes. This provides versatility to researchers to simulate different types of rock masses when studying the capacity of different support elements.

However, until recently, there have been significant limitations in terms of the spatial resolution used to determine the specific load transfer mechanisms being measured for an embedded rock bolt. Through the use of a Rayleigh Optical Frequency Domain Reflectometry (ROFDR) technique, (Forbes et al. 2017) and Cruz (2017), and Vlachopoulos et al. (2018), were able to use a single Fiber Optic Sensor (FOS) to examine the axial strain along a FGRB at a spatial resolution of 0.65 mm. This virtually continuous strain monitoring technique provides comprehensive insight into the of the load transfer mechanism(s) to date with a wider view of determining the overall rock bolt behaviour and performance. This allows for in-depth geomechanical insight with respect to the behaviour of fully grouted rock bolts with a view to optimizing the performance of such rock support elements.

3 EXPERIMENTAL PROCEDURE

A series of five pull-out tests were conducted within the structures laboratory at the Royal Military College (RMC) in order to investigate the mechanistic response of a FGRB; both along the rebar and the steel pipe (simulated rock) along with the radial stiffness generated during co-axial loading. The five samples were all cement-based FGRB with varying embedment lengths, see Table 1.

Table 1. Specimen details for the five fully grouted rock bolt elements that were tested as part of this stage of the broader research program / investigation.

Serial	Support Element	Embedment Length (mm)	Borehole Diameter (mm)
1	Rebar 19 mm Gr. 60 DSI	100	40.9 1 ½ Sch 40 Steel A53
2		250	
3		500	
4		750	
5		1000	

For all pull-out tests, the rock mass was simulated by a 1 ½ schedule 40 steel pipe which has a radial confinement of 1600 MPa/mm. According to Hyett et al. (1992) and Gercek (2007), this is consistent with in-situ granite.

3.1 Specimen Preparation

Lengths of 19 mm diameter rebar were cut to allow co-axial response of the sample by having free length of rebar on either end of the specimen. The rebar sections were then modified with three 2.5 mm by 2.5 mm machined grooves orientated 120 degrees from one another. These grooves housed the Fiber Optic Sensors (FOS), see Figure 5. The grooves were cleaned, and the FOS were installed and bonded to the rebar using a metal bonding adhesive which also provided a layer of protection to the sensor as discussed by Forbes et al. (2017).

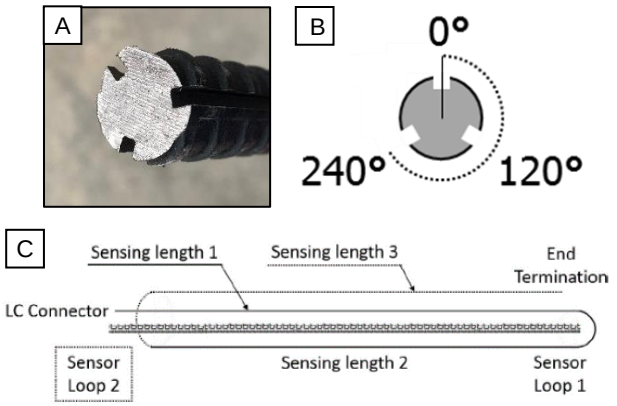

Figure 5. (A) Modified rebar sample with three machined grooves for FOS. (B) schematic of the orientation of the three machined grooves (C) schematic of the FOS lengths along the rebar (modified after Forbes et al. 2017).

Once the FOS were installed, the samples were grouted using general purpose portland limestone cement with a 0.4 water/cement (w/c) ratio. The 100 mm and 250 mm samples were grouted from the top due to their short embedment lengths while the longer three lengths were grouted from the bottom through a threaded brass fitting installed near the bottom of the pipe (see Figure 6). Grouting from the bottom was used in order to prevent pockets of air from forming which would have negatively affected the consistency and capacity of the grout. Each sample was capped on the top and bottom with a 1 ½ ABS pipe cap with a center hole to secure the rebar while the grout cured (see Figure 6).

Once the samples cured, the corrosive protected coating was removed to allow effective bonding between the pipe and the monitoring equipment, see **Error! Reference source not found.**. The exterior monitoring system comprised of discrete (strain gauges) and distributed (FOS) sensing systems. Both systems measured radial strain on the pipe (simulated rock). Each sample was outfitted with 1, 2 or 3 rings of strain gauges spaced evening along the length of the rebar. Each ring contained three strain gauges spaced evening around the circumference of the pipe, see **Error! Reference source not found.** and Table 2.

Table 2. Strain gauge details for all five samples.

Sample	No. of Strain Gauge Rings	Total No. of Strain Gauges
100 mm	1	3
250 mm	2	6
500 mm	3	9
750 mm	3	9
1000 mm	3	9

In addition to the strain gauges, loops of FOS were also installed evenly along the entire length of the steel pipe. The FOS were also measuring radial strain and the spacing of the loops varied between the five samples in order to determine the optimal spatial resolution, see Table 3. The FOS loops were horizontal and evenly spaced along the specimen with FOS connections running between the loops, see Figure 9. The FOS were bonded to the steel pipe using structural epoxy adhesive. The ends of the FOS were also protected using heat shrink tubing, see **Error! Reference source not found.**. Both the FOS around the pipe and along the rebar allow for a spatial resolution of 0.65 mm which provides virtually continuous measurements along two major components of the FGRB load transfer system.

Figure 7. Top – After the corrosion protection coating has been removed. Bottom – Prior to sample preparation.

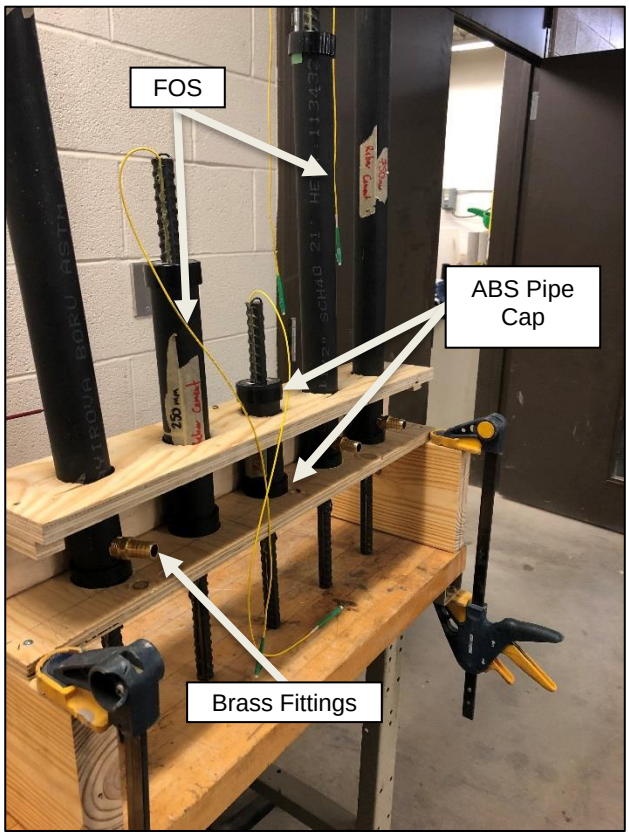

Figure 6. Five grouted samples during the curing process.

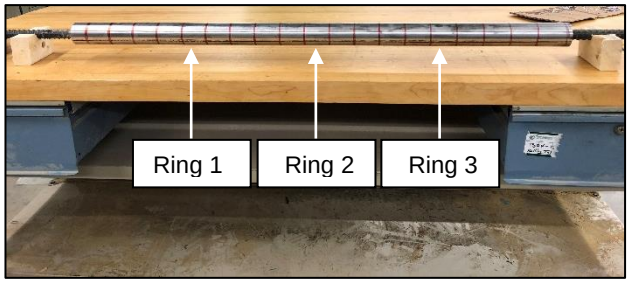

Figure 8. Location of the three rings of strain gauges along 1000 mm sample.

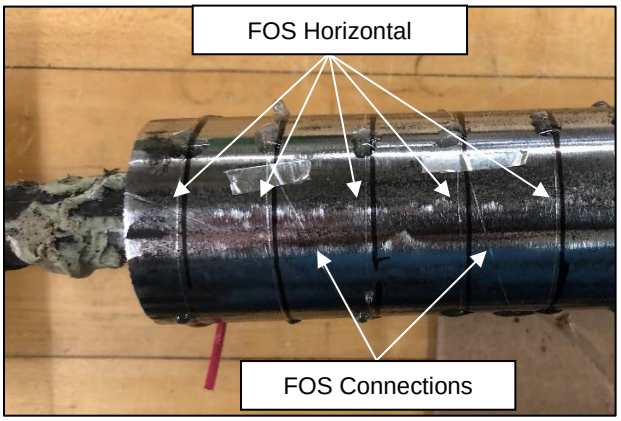

Figure 9. FOS horizontal loops and FOS connections along 500 mm sample.

Table 3. FOS details on steel pipe

Sample	No. FOS Loops	FOS Loop Spacing (mm)
100 mm	1	3
250 mm	2	6
500 mm	3	9
750 mm	3	9
1000 mm	3	9

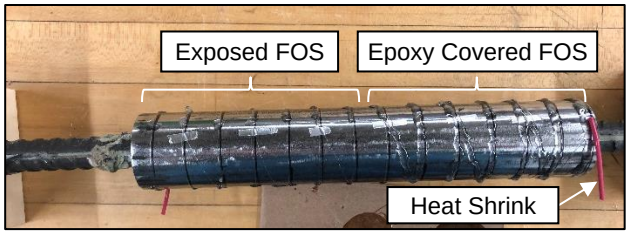

Figure 10. 250 mm sample with both exposed FOS and epoxy covered FOS.

3.2 Pull-out Testing Procedure

The pull-out test was carried out using a 322.41 Material testing System (MTS) with an MTS hydraulic actuator and an MTS Series 661 Force Transducer with a capacity of 500 kN. The MTS machine was outfitted with hydraulic grips with a "V" cut that was designed for 19 mm rebar. The sample was placed between two 25.4 mm (1 inch) steel plates connected by six 19.1 mm (¾ inch) threaded bars which restricted sample displacement during axial loading, see Figure 11.

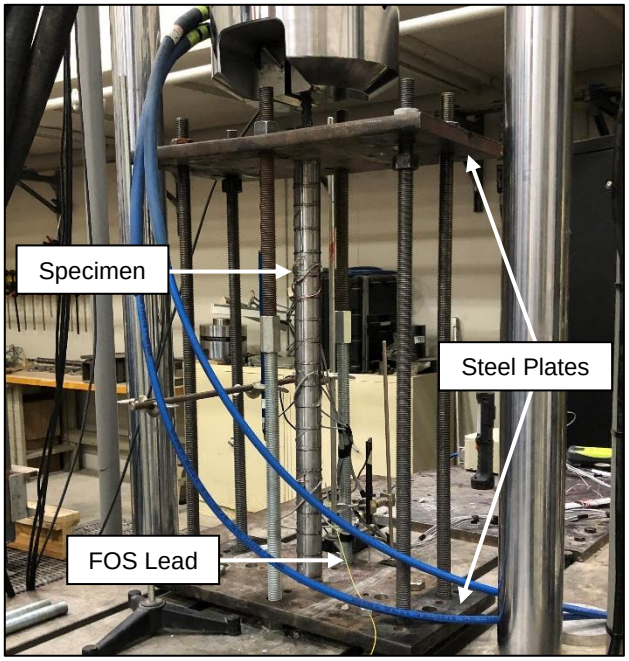

Figure 11. Pull-out test set-up.

Two 200 mm Linear Voltage Differential Transformer (LVDT), and one 100 mm LVDT monitored the overall specimen displacement. One LVDT was measuring the displacement of the free rebar at the unloaded end. The second and third LVDTs were measuring the displacement of the top and bottom plates respectively, see Figure 12. All strain gauges, LVDTs, hydraulic actuator, and load cell were connected to a Hottinger Baldwin Messtechnik (HBM) MGCplus data acquisition unit (DAQ) which logged all measurements at a rate of 1 Hz. The FOS on the pipe and rebar were connected to separate Luna ODiSI-B Optical Fiber Interrogrators and captured measurements at a rate of 1 Hz.

The samples were tested using displacement control loading of 1 mm/min until the FOS were broken at around 2% strain, then the loading was increased to 5 mm/min until the grout or the rebar failed.

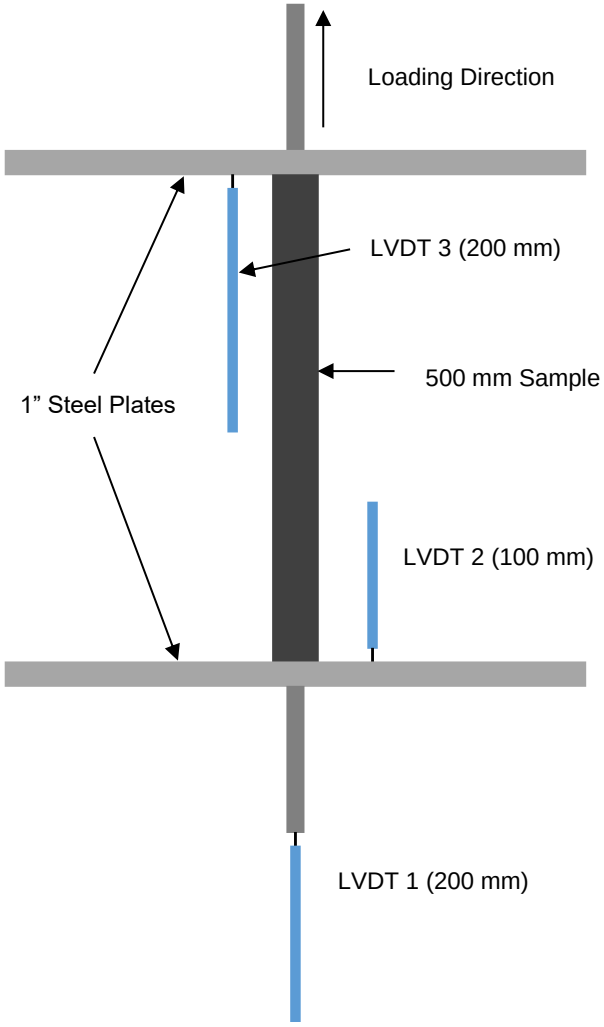

Figure 12. Layout of LVDTs during testing.

4 SELECTED RESULTS

Each sample underwent the same loading procedure. Note that only the results associated with one of the five samples, the 500 mm sample, will be examined and presented within this paper.**Error! Reference source not found.** Figure 13, illustrates the loading for the 500 mm sample. Highlighted at 115 kN (point 1) is the position where the displacement rate was increased to 5 mm/min (after the failure of the FOS along the rebar). The load values were taken directly from the load actuator via the HBM MGCplus DAQ unit and the displacement values were calculated based on the difference between the LVDT 1 (unloading end of the sample), and LVDT 2 and 3 (top and bottom steel plates), see Figure 12 for LVDT layout.

The strain on the rebar is presented up to 110 kN at 10 kN intervals, as seen in Figure 14 as shortly afterwards the FOS reached its maximum strain of 1.5%. When the FOS on the rebar failed, only ~65% of the embedded rebar was activated which equates to 0.35 m of rebar.

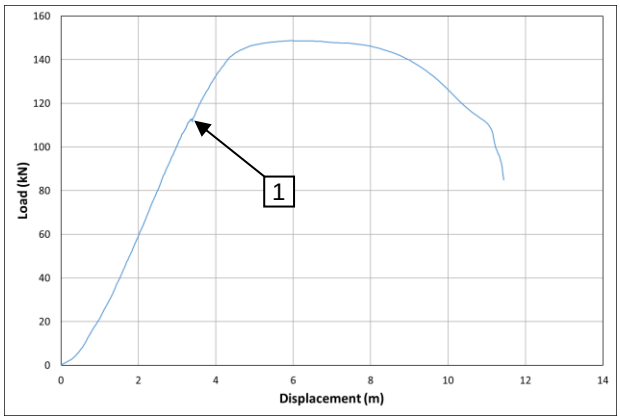

Figure 13. 500 mm Sample - Load Displacement Diagram. Point 1 – failure of the FOS along the rebar. Adjusted displacement rate to 5 mm/min.

FOS were also installed around the pipe to capture the radial load transfer from the rebar to the pipe (i.e. simulated rock and confinement) via strain measurements. Figure 15 depicts the results obtained with respect to the strain along the FOS. The first 1.25 m of FOS was not attached to the pipe and was used to connect to the analyzer. Each 'valley' indicates a horizontal loop of FOS and the peaks are associated with the connections between the FOS loops. Figure 16 depicts the captured strains along the FOS loop around the steel pipe (i.e. surrounding rock mass and confinement simulation) at 130 kN load.

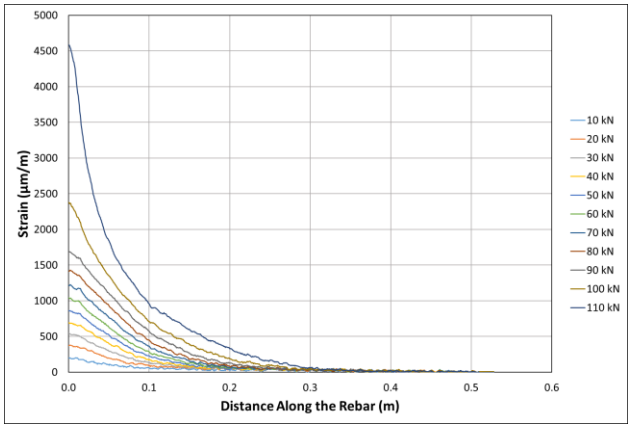

Figure 14. FOS strain measurements along the rebar.

The strain measurements were then averaged for each of the loops and graphed in terms of length along rebar, see Figure 17. These strain measurements provide insight into the load transfer mechanism for the entire loading sequence. These results are of particular importance for high loads since the FOS along the rebar failed at ~115 kN. One can see that the entire rebar quickly activated between 110 kN and 120 kN. The first measurement for 90 kN (0.05 m from loading end along the rebar) to 140 kN is much lower than other comparable points. This can be attributed to the grout shear failure that left a conical void at the loading end and no longer transferring load to the pipe. The grout is allowed to vacate the pipe due to the 1 inch steel plate bending at higher loads, creating a void to allow the grout to burst outwards, see Figure 18.

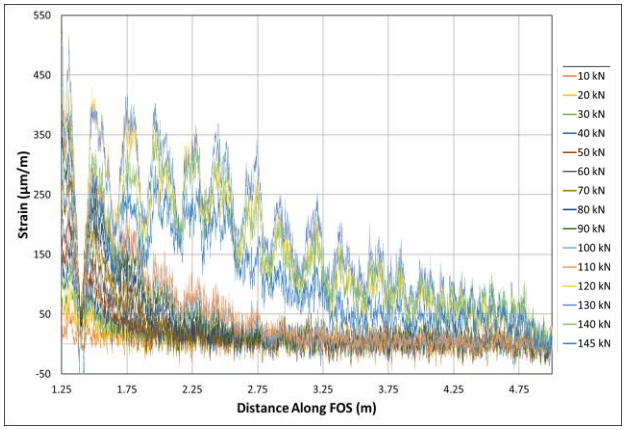

Figure 15. FOS strain measurements on steel pipe.

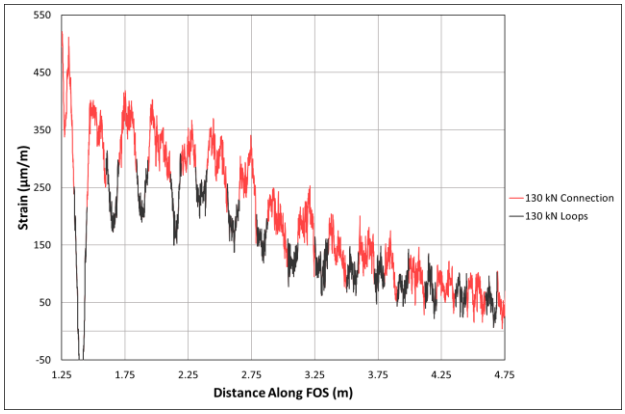

Figure 16. FOS strain measurements on steel pipe for 130 kN. Highlighting FOS loops and connections.

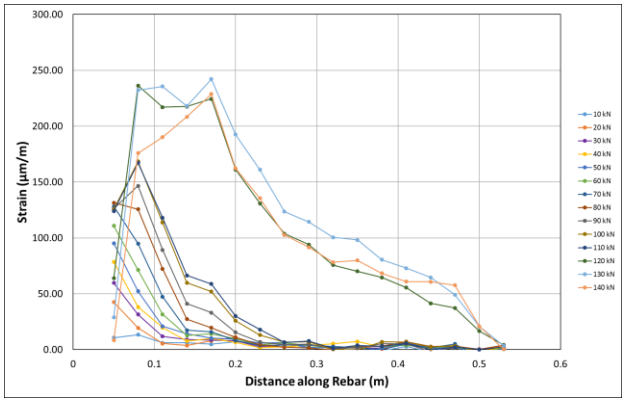

Figure 17. Average FOS strain measurements on steel pipe.

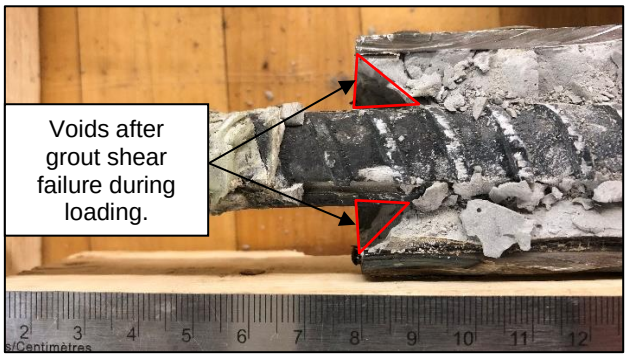

Figure 18. 500 mm sample highlighting grout shear failure during loading.

Comparing Figure 14 and 17, it allows one to interpret, with relative certainty, the load characteristics of the rebar system based on the load being transferred to the pipe. This correlation may allow monitoring at much high loads, where previous tests using FOS were unable to monitor at such load levels.

The strain measurements on the steel pipe between the FOS and strain gauges were also compared. The 3 (external pipe) rings of strain gauges were compared against the nearest (external pipe) FOS loop and the coefficient of correlation, R, and coefficient of determination, R^2, were calculated as seen in Table 4.

Table 4. 500 mm sample – coefficients of correlation, R, and determination, R^2, for each ring of strain gauges.

	Ring 1	Ring 2	Ring 3
Distance along Pipe (m)	0.13	0.26	0.38
Coeff. Of Correlation, R	0.46	0.66	0.84
Coeff. Of Determination, R^2	0.21	0.44	0.71

The low R and R^2 values for ring 1 and ring 2 can be attributed to two factors: First, rings 1 and 2 only had two functioning strain gauges while ring 3 had all three strain gauges functioning properly. The malfunctioning strain gauge on both ring 1 and ring two had a significant effect when calculating the hoop strain of the pipe. Lastly, the FOS loops that were used in comparison were 1-2 cm away from the strain gauges, which lead to different values. Further tests within the overall research program will be conducted in order to determine how to more accurately compare the strain measurements between FOS and strain gauges on the steel pipe.

4.1 Post-test Inspection

After the testing was complete on all specimens, a forensic analysis was conducted to determine:

1. Quality of the grout;

2. Confirm mode of failure; and,

3. Any other factors that may provide insight into quality control and system behaviour.

As seen in Figure 19, the grout was evenly distributed throughout the sample with very little signs of air pockets which would have negatively affected the strength of the grout. After visual inspection of the rebar, grout shearing about the asperities and their periphery at the grout/rebar and grout interface. was determined to be the dominate mode of failure, Figure 20.

Figure 19. Minor air pockets for 500 mm sample.

Figure 20. Top. 500 mm sample cut diametrically. Bottom - Center of 500 mm sample illustrating grout shearing.

5 CONCLUSION

The mechanical response of an axially loaded FGRB is complex and requires specific techniques in order to accurately capture such behaviour(s). Through the use of state-of-the-art FOS strain measuring instrumentation technique that was developed at the Royal Military College of Canada, a virtuously continuous monitoring plan can be implemented with regards to grouted rock bolts (rebar). Placing FOS on the steel pipe in addition to the rebar not only provided a more complete picture of the load transfer mechanisms but also captures the system behaviour associated with the entire loading sequence (by strain measurements) at much higher loads; this is currently a limitation of installing FOS solely along the rebar. A better understanding the load transfer mechanisms at the point of failure may also lead to a better understanding of the specific geomechanisms at play which will ultimately provide insight into a more optimized designed based off of critical embedment lengths.

Future tests will also focus on determining the effect on critical embedment length based on different grout types (i.e. cement and grout) as well as examining the specific axial responses of the rebar support system based on varying confinement stresses (i.e. rock types). Installing FOS on multiple components of the support system are critical to the success of both of these investigations.

6 ACKNOWLEDGMENTS

The authors would like to thank the Royal Military College (RMC), RMC Green Team, the Department of National Defence (DND), and YieldPoint Inc. for supporting this research.

7 REFERENCES

Benmokrane, B., Chennouf, A., and Mitri, H.S. 1995. Laboratory evaluation of cement-based grouts and grouted rock anchors. International Journal of Rock Mechanics and Mining Sciences and, 32(7): 633–642.

Charette, F., and Bennett, A. 2017. The importance of the face plate as part of an engineered holistic ground support scheme in dynamic conditions. Proceedings of the Eighth International Conference on Deep and High Stress Mining, Deep Mining 2017, (2012): 709–722.

Cruz, D., Vlachopoulos, N., and Forbes, B. 2016. The Geo - Mechanical Response of Axially Loaded Rock Bolts using Fiber Optic Technology Respuesta Geo - Mecánica de Pernos de Anclaje Cargados Axialmente utilizando Tecnología de Fibra Óptica.

Cruz, D.F. 2017. The Geomechanical Response Of Axially Loaded Fully Grouted Rock Bolts Utilizing Fibre Optics Technology.

Forbes, B., Vlachopoulos, N., Diedrichs, M.S. (2018, September). The Application of Distributed Optical Strain Sensing (DOS) to Optimize Underground Support Design. Research Seminar presented at the 71st Canadian Geotechnical Conference, GeoEdmonton 2018, Edmonton, Alberta.

Forbes, B., Vlachopoulos, N., Hyett, A.J., and Diederichs, M.S. 2017. A new optical sensing technique for monitoring shear of rock bolts. Tunnelling and Underground Space Technology, 66(October 2016): 34–46. Elsevier.

Gercek, H. 2007. Poisson's ratio values for rocks. International Journal of Rock Mechanics and Mining Sciences, 44(1): 1–13.

Hyett, A.J., Bawden, W.F., and Reichert, R.D. 1992. The effect of rock mass confinement on the bond strength of fully grouted cable bolts. International Journal of Rock Mechanics and Mining Sciences and, 29(5): 503–524.

Kikkawa, N., Itoh, K., Hori, T., Toyosawa, Y., and Orense, R.P. 2015. Analysis of labour accidents in tunnel construction and introduction of prevention measures. : 517–521.

Li, C. 2007. A Practical Problem with Threaded Rebar Bolts in Reinforcing Largely Deformed Rock Masses Technical Note A Practical Problem with Threaded Rebar Bolts in Reinforcing Largely Deformed Rock Masses.

Li, C., and Stillborg, B. 1999. Analytical models for rock bolts. International Journal of Rock Mechanics and Mining Sciences, 36(8): 1013–1029.

Mark, C., Compton, C., Oyler, D., and Dolinar, D.R. 2002a. Anchorage Pull Testing for Fully Grouted Roof Bolts. Proceedings of the 21st International Conference on Ground Control in Mining: 105–113.

Mark, C., Compton, C., Oyler, D., and Dolinar, D.R. 2002b. Anchorage Pull Testing for Fully Grouted Roof Bolts. Proceedings of the 21st International Conference on Ground Control in Mining, (figure 1): 105–113.

Vlachopoulos, N., Cruz, D., and Forbes, B. 2018. Utilizing a novel fiber optic technology to capture the axial responses of fully grouted rock bolts. Journal of Rock Mechanics and Geotechnical Engineering, 10(2): 222–235.

Windsor, C.R. 1997. Rock reinforcement systems. International Journal of Rock Mechanics and Mining Sciences, 34(6): 919–951.